Solar Energy Materials & Solar Cells 94 (2010) 830–835

Contents lists available at ScienceDirect

Solar Energy Materials & Solar Cells

journal homepage: www.elsevier.com/locate/solmat

Modeling, geometric optimization and isolation of the edge region in silicon solar cells

Daniel Kray *,[1]

Innovalight, Inc., 965 East Arques Avenue, Sunnyvale, CA 94085, USA

ARTICLE INFO

Article history:
Received 14 July 2009
Received in revised form
30 December 2009
Accepted 31 December 2009
Available online 19 February 2010

Keywords:
Solar cell
Edge isolation
Simulation
Laser
Resistance-limited enhanced recombination
Analytical modeling

ABSTRACT

Commercial front-contact solar cells can often be represented as an equivalent circuit with two diodes. A first diode models low-level injection Shockley-Read-Hall recombination in the bulk of the solar cell and associated with an ideality factor of one, while the second diode models several loss mechanisms as depletion region recombination or edge recombination. The ideality factor of the second diode is most often greater than one, and in the case of edge recombination a value of two is observed in many cases. Even values above two can be explained by e.g. coupled defect level recombination [10]. As the associated impact of the second diode on the *IV* curve of a solar cell is generally strong, an optimization of the edge region is sought. This can be done through minimizing the dark saturation current of the edge as well as by geometrical optimization of the grid and edge isolation groove. In this paper, an equivalent circuit model for the edge region of a solar cell with full-area rear contact and H-grid front contacts is presented. Using approximations for the short-circuit current in the edge region, which are derived from numerical simulations, the model allows for the extraction of dark-saturation currents as well as for geometrical grid optimization. After validation of the model on experimental data, projections are made on a variety of solar cells, pointing out the influence of the edge design on the overall cell performance.

© 2010 Elsevier B.V. All rights reserved.

1. Introduction

It is known that by optimizing the design of the edge area of the solar cell (i.e. the region beyond the front metal fingers), the efficiency can be increased. It is believed that any effect to the cell manufacturing cost would be minimal, since the proposed optimization would make use of existing capital equipment and would not require costly process changes. Thus this paper investigates the modeling of the edge region and shows the impact of different geometric designs and isolation qualities.

In general, the edge area contains the physical wafer edge with the intersected front pn junction. It is known [1–4] that this area also tends to increase charge carrier recombination that can severely impact on the device efficiency (by deforming the *IV* curve at lower voltages). In a conventional front-contact solar cell, increased recombination is associated with edge isolation (most often achieved via laser grooving), which tends to be located close to the wafer edge in order to maximize surface area for current generation. In general, the electrical coupling of this increased recombination region to the main body of the solar cell may be modeled as a resistor whose resistance depends on the geometry of the edge region and the front contacts. Depending on the dark saturation current of the edge groove, the emitter sheet resistance, the bulk doping, the current generation outside the isolation groove and the wafer thickness, the optimum distance of the front contacts to the wafer edge can be calculated.

To accomplish this task, an equivalent circuit of the solar cell is given in this paper and an analytical model is proposed to determine the series resistance associated with the edge current flow. Together with estimations for the edge current generation, derived from one-dimensional numerical simulations, the optimum finger distance to the edge can be calculated (cf. Fig. 1).

2. Modeling the edge region

To model the impact of the edge region on the overall performance of the solar cell, the equivalent circuit in Fig. 2 is used, based on the resistance-limited enhanced recombination model [7]. The main body of the solar cell is represented by a diode with ideality 1, a current source and a resistor that accounts for the series resistance in the bulk and the emitter. In parallel to the main body, the edge region is represented by two diodes (the first one being identical to the main body diode), a current source, a shunt resistor and a series resistor that accounts for the series resistance associated with majority current flow through the edge region. The external resistor finally represents the non-bulk series

* Tel.: +1 408 419 4469; fax: +1 408 419 4758.
E-mail addresses: dkray@innovalight.com, daniel.kray@rena.com.
[1] Now with Rena GmbH, Ob der Eck 5, 78148 Gütenbach, Germany, Tel.: +49 761 1563794 15.

0927-0248/$ - see front matter © 2010 Elsevier B.V. All rights reserved.
doi:10.1016/j.solmat.2009.12.033

resistance contributions from the current flow through bulk metals as well as contact resistances for instance. In an industrial solar cell with decent efficiency, the shunt resistance and the second diode are mainly dominated by the edge influence, thus they are not represented in the main body of the solar cell. The model could be extended by these elements but the increased number of fit parameters does complicate the fit procedure and the result interpretation.

2.1. Estimation of the edge current generation

In the presented model, the edge region is divided into 3 different parts as illustrated by Fig. 3. To estimate the current generation in those regions, the one-dimensional simulation program PC1D [5] is used. First, a baseline model for an 18% efficient solar cell as manufactured by Innovalight [6] was set up. To determine J_{sc} for the edge regions 1, 2 and 3, the following assumptions are made: As the emitter outside the edge isolation groove is directly connected to the rear *Al* contact, it is a shunted floating junction that is known to provide very little passivation [7,8]. Thus, the PC1D baseline model is used with very high front and/or rear surface recombination velocity (S=1e7 cm/s) and accounting for the removed metal shading (a value of 8% is used) in the edge region. These calculations led to the following relative current generation where 100% corresponds to the J_{sc} of the main solar cell:

- Region 1 (S_{front}=S_{rear}=1e7 cm/s, no shading): 54%
- Region 2 (S_{front}=same as main cell, S_{rear}=1e7 cm/s, no shading): 101%
- Region 3 (S_{front}, S_{rear}=same as main cell, no shading): 109%

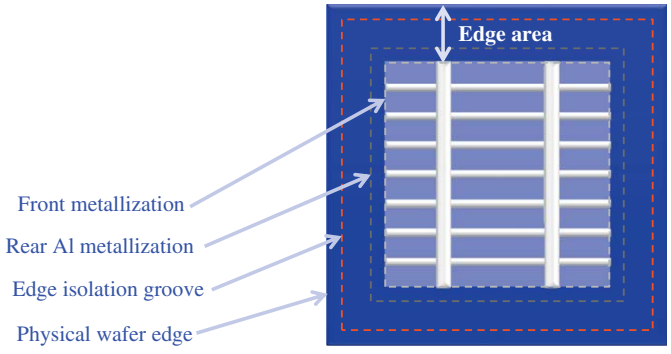

Fig. 1. Definition of the edge area for a conventional solar cell with full area *Al*-BSF rear side and front laser edge isolation.

For region 1 however, the baseline model with absent front and rear passivation overestimates the actual current generation as in this region the bulk recombination is also strongly increased via the physical wafer edge with very little passivation. We estimate the relative current collection there to be ~11% as derived from fitting the presented model to measured *IV* curves. Details on this are shown in the experimental validation section.

In the edge model, the area-weighted average of these relative J_{sc} numbers is used for the optimization calculations:

$$j_{L,edge} = \frac{1}{A_1+A_2+A_3}(A_1 j_{sc,1} + A_2 j_{sc,2} + A_3 j_{sc,3})$$

While A_i and $j_{sc,i}$ denote the area and short-circuit current density of region i. We approximate the light-generated current by the short circuit current.

2.2. Analytic calculation of the edge series resistance

In order to determine the series resistance of the edge region, the method for calculation of distributed series resistance, as described in [9] is used. For this we consider the majority current flow paths that we assume to be purely lateral or vertical as indicated in Fig. 3. The only exception to this is the consideration of the spreading resistance in the front emitter due to the grid pattern. These assumptions allows for the analytical calculation of the lumped series resistance $R_{ser,edge}$ that we use in the circuit model. The resulting formulas for the different carrier types and regions are somewhat lengthy and can be found in the appendix.

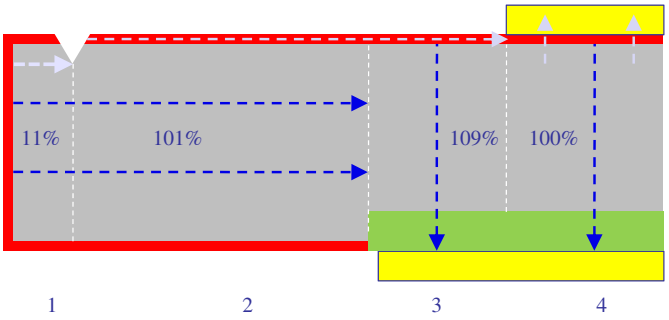

Fig. 3. Different regions of a solar cell used in the proposed model: (1) outside the edge isolation groove, (2) outside the rear *Al*-BSF, (3) outside the front metallization, (4) main solar cell. The numbers represent the assumed current generation relative to the main solar cell as derived by numerical simulations. The dark (light) blue arrows indicate hole (electron) current flow directions assumed for the respective areas. (For interpretation of the references to color in this figure legend, the reader is referred to the web version of this article.)

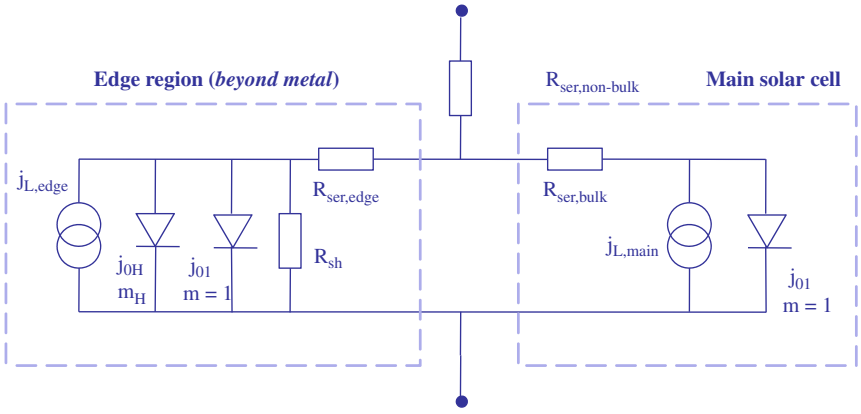

Fig. 2. Equivalent circuit model for solar cell with edge region, a variation of resistance-limited enhanced recombination [7].

2.3. Validation of the model

Industrial solar cells of 125×125 mm^2 size and different edge isolation schemes have been fabricated at the Innovalight pilot line and their light *IV* curves have been measured. From the light *IV* curve, the associated *m*–V curve [7] has been derived—*m* representing the local ideality factor that shows more details of the curve shape. In this study, the light *IV* curve has been favored compared to the dark *IV* since in the illuminated case, more carriers are generated in the edge region and a higher voltage drop at the edge series resistance can be expected compared to the dark case where the current is injected in the device, avoiding high series resistance regions.

The J_{sc} and series resistance model as well as the network simulation have been implemented in a spreadsheet so that a fit of the model parameters to experimental light *IV* and light *m*–V curves was possible. Four different cell types from two cell batches have been used in the validation as shown in Table 1. The full set of *IV* parameters is not discussed here as the baseline process improved in between the different batches but it is noted that the observed impact of improved edge isolation on the same batch is in the order of 0.2–0.3%$_{abs}$.

For the fit procedure, as many measured parameters as possible were used for the model. These were J_{sc} (starting value for $J_{L,main}$), R_{sh}, the grid and the edge geometry. J_{01} was fitted to the higher voltage region to give the correct V_{oc}.

As it was possible to fit cells that only differed in their distance of the edge isolation groove to the wafer edge or in the used laser process by simply adjusting the single corresponding model parameter, we feel confident that the model is suited for predicting trends and give as accurate numbers as can be expected from a simple analytical model. Interestingly, the model data extracted for the plasma edge isolation clearly show an increased current generation in region 1 (the region outside the isolation 'groove') $J_{sc,1}$. This is due to the fact that the plasma process removes the shunted emitter from parts of the edge and these areas are then passivated by the front SiN_x. On the other hand, the current generation in region 1 for the laser-isolated cells was determined to be much lower than anticipated from PC1D simulations. Instead of around 54% (as calculated from the baseline cell model with $S_{front}=S_{back}=1e7$ cm/s), only about 11% of the current of the main solar cell is generated. This shows the very low passivation quality of the shunted edge emitter.

An example of a model fit to experimental data is shown in Fig. 4. For the fit of the light *IV* curve of this cell, the varied parameters were $J_{sc,main}$ (set to measured J_{sc}+0.1 mA/cm^2), j_{01}, $R_{ser,non\text{-}bulk}$ and j_{0H}. As the latter 3 parameters impact on the shape of the *IV* and m–V curve in very different ways, an independent optimization was possible. The results for the model calculations compared to the measured *IV* parameters are shown in Table 2. From the performance data of the edge and main solar cell it

Table 2
Model fit results compared to light *IV* measurement.

Cell	V_{oc} [mV]	J_{sc} [mA/cm^2]	*FF*	Efficiency [%]
Edge cell	531	32.9	0.672	11.8
Main cell	628	36.6	0.810	18.6
Edge+main cell	623	36.5	0.789	17.9
Edge+main cell+$R_{ser,non\text{-}bulk}$	623	36.5	0.784	17.8
Measurement	*623*	*36.5*	*0.784*	*17.8*

Table 1
Cell types used to validate edge region model and comparison of extracted dark saturation current densities to literature data. $J_{sc,1}$ ($J_{sc,edge}$) denotes the short circuit current density outside the edge isolation groove (of the whole edge region) in relation to the main body of the solar cell. The distance of the plasma edge isolation to the edge has been extracted from the model fit. Values from literature are shown for comparison.

Batch #	Edge isolation type	Laser parameters	Distance of edge isolation groove to wafer edge [μm]	$J_{sc,1}$ [%$_{rel}$]	$J_{sc,edge}$ [%$_{rel}$]	$R_{ser,edge}$ [Ω cm^2]	J_{0H} [A/cm]
2797	Laser	A	125	11	90	0.31	1.15e−7
2395	Laser	B	125	11	90	0.31	1.40e−7
2395	Laser	B	250	11	80	0.30	1.40e−7
2395	Plasma	–	*50*	33	97	0.33	1.70e−7
From [7]	Laser	Extra damaging					5.6e−7
From [4]	Laser						1.9e−8
From [4]	Laser+NaOH						1.72e−9
From [2]	Laser+cleave	Edge cleaving					1.3e−8

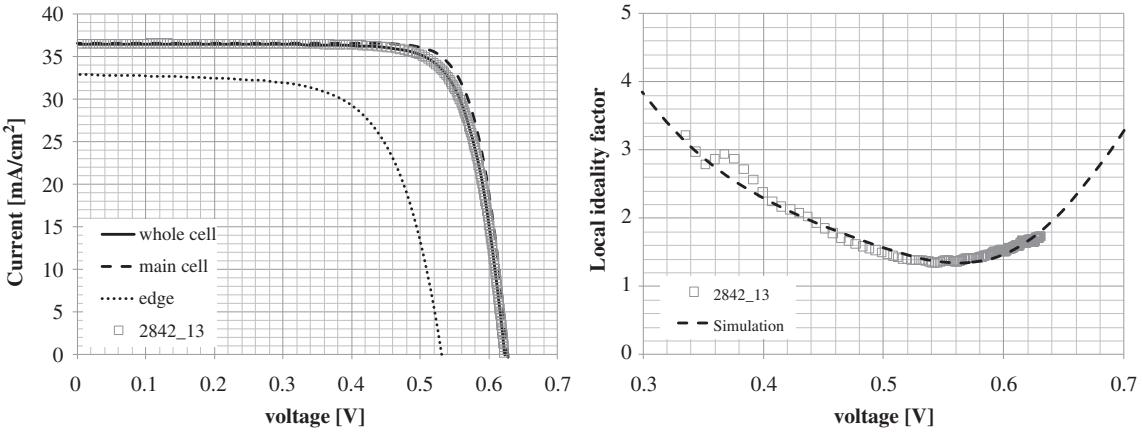

Fig. 4. Example of fitting the circuit model to experimental data.

becomes obvious that the edge strongly impacts the global cell performance: The 17.8% efficient solar cell consists basically of a main body with 18.6% efficiency that is connected in parallel to an 11.8% efficient edge solar cell. While the impact on V_{oc} and J_{sc} is minor, the fill factor is strongly affected by the edge region.

3. Optimizing the edge region

After the experimental validation of the model, it is used to optimize the edge region and to predict the optimization potential depending on main cell parameters. One obvious optimization strategy is to move the edge isolation groove as close to the edge as possible in order to reduce the low J_{sc} region. This is constrained by the accuracy of the laser system and the need for process stability with variation in wafer geometry. In the following we assumed a conservative number of 200 μm.

3.1. Optimum finger length

The geometrical optimization of the edge region is sought by varying the distance of the finger tips to the wafer edge x_e. For the sake of simplicity, the distance of the *Al* rear contact to the edge is set to the same value and varied accordingly. In principle, using longer fingers that extend closer to the edge has different aspects for cell performance:

- Introducing more shading to the edge region → reduction of J_{sc}
- Reducing the edge series resistance losses → increase in *FF*
- Better coupling of the increased edge recombination to main solar cell → decrease in *FF*
- Extending the rear *Al*-BSF passivated areas → increase in V_{oc} and J_{sc}

Obviously, there are convoluted effects that make a careful optimization necessary. The result will depend on cell parameters as the base doping level, the emitter sheet resistance, the current generation outside the edge isolation groove ($J_{sc,1}$) and the wafer thickness. For this study, the model was used to calculate cell performance for the following parameter range:

- Wafer edge length: 125 mm (square)
- Shunt resistance: 5000 Ω cm^2
- Base resistivity: 1 or 10 Ω cm
- Emitter sheet resistance: 50, 100 or 300 Ω/square (assuming j_{0e} of 400, 100 or 30 fA/cm^2 and finger spacing of 3.0, 2.5 or 1.65 mm, respectively, 130 μm wide fingers)
- Wafer thickness: 50 or 200 μm (assuming j_{0b} of 1040/1220 fA/cm^2 for 50 μm thickness on 1/10 Ω cm and of 659/1160 fA/cm^2 for 200 μm thickness on 1/10 Ω cm)
- Main solar cell short circuit current density $J_{sc,main}$: 36/37 mA/cm^2 for 50/200 μm thickness
- Relative short circuit current density outside edge isolation groove $J_{sc,1}$: 10 or 75%
- Edge diode saturation current density J_{0H}: 1, 3, 10 or 30e−8 A/cm with m_H=2
- Distance of finger tips and *Al* rear contact to the edge: 300 to 1000 μm in steps of 100 μm.

The results of the model calculations are summarized in Table 3. The relative difference in efficiency for the variation range of x_e as well as the optimum value for x_e are shown. In principle it can be stated that the optimization of x_e is a minor optimization task for most practical cases. A relative efficiency difference of 0.5% in the table would translate to a potential of ~0.1% absolute efficiency gain due to optimization of x_e. Those parameter sets are highlighted by red font color in the table. In order to give this optimization task reasonable importance, either a very high emitter sheet resistance on 1 Ω cm or a very low cell thickness (50 μm) on lowly doped material must be present. Both cases are not yet relevant for industrial solar cells. To choose nevertheless the optimum value of x_e, general rules can be

Table 3
Model calculations for varying cell parameters. The relative difference in efficiency when changing the distance of the finger tips x_e and the *Al* rear contact to the wafer edge has been calculated as well as the optimum value of x_e. The variables are the bulk resistivity, the emitter sheet resistance, the cell thickness, the J_{sc} outside the edge isolation groove (J_{sc1}) and the dark saturation current density of the edge region (J_{0H}). For more details, see text.

P_b [Ω cm]	P_{sheet} [Ω/square]	J_{0H} [1e-8 A/cm]→		Relative efficiency difference for $x_e \in$ [300,1000 μm]				Optimum value for x_e			
		W [μm]	J_{sc1} [%]	1	3	10	30	1	3	10	30
1	50	50	10	0.08%	0.10%	0.10%	0.18%	300	300	300	1000
1	50	50	75	0.10%	0.13%	0.18%	0.12%	300	300	300	300
1	50	200	10	0.07%	0.08%	0.09%	0.07%	300	300	300	1000
1	50	200	75	0.08%	0.10%	0.16%	0.20%	300	300	300	300
1	100	50	10	0.06%	0.09%	0.09%	0.45%	300	300	300	1000
1	100	50	75	0.08%	0.13%	0.19%	0.31%	300	300	300	1000
1	100	200	10	0.05%	0.08%	0.07%	0.25%	300	300	300	1000
1	100	200	75	0.06%	0.11%	0.31%	0.23%	300	300	300	300
1	300	50	10	0.06%	0.12%	0.11%	0.87%	600	500	600	1000
1	300	50	75	0.11%	0.20%	0.24%	0.60%	500	300	300	1000
1	300	200	10	0.06%	0.12%	0.20%	0.85%	600	500	800	1000
1	300	200	75	0.10%	0.19%	0.15%	0.57%	500	300	700	1000
10	50	50	10	0.24%	0.32%	0.22%	1.27%	300	300	600	1000
10	50	50	75	0.40%	0.52%	0.46%	0.84%	300	300	300	1000
10	50	200	10	0.08%	0.12%	0.13%	0.28%	300	300	300	1000
10	50	200	75	0.12%	0.18%	0.24%	0.13%	300	300	300	900
10	100	50	10	0.22%	0.31%	0.22%	1.34%	300	300	600	1000
10	100	50	75	0.39%	0.52%	0.46%	0.82%	300	300	300	1000
10	100	200	10	0.06%	0.11%	0.12%	0.37%	300	300	300	1000
10	100	200	75	0.10%	0.18%	0.25%	0.18%	300	300	300	1000
10	300	50	10	0.24%	0.35%	0.26%	1.44%	400	400	600	1000
10	300	50	75	0.44%	0.60%	0.51%	0.86%	300	300	300	900
10	300	200	10	0.07%	0.15%	0.16%	0.61%	600	500	600	1000
10	300	200	75	0.13%	0.25%	0.33%	0.31%	500	300	300	1000

formulated:

- If j_{0H} is elevated ($\geq 3e-7$ A/cm) use short fingers (high value for x_e) unless the edge is well passivated and the local current generation is high.
- If j_{0H} is low ($\leq 1e-7$ A/cm) use long fingers

Superimposed to those are technical constraints concerning pattern alignment and accuracy that should have higher priority since alignment failure may have serious impact on device performance and machine uptime.

3.2. Optimizing distance of laser groove to the edge

Region 1 in Fig. 3 is clearly the lowest performing region of the edge, so the reduction of its size is sought by moving the edge isolation groove as close to the edge as possible. The impact of this optimization is a nearly linear increase in current with negligible impact on *FF*. This effect is shown in Fig. 5 for good (j_{0H}=1e−7 A/cm) and bad (j_{0H}=3e−7 A/cm) laser parameters as calculated with the presented model. A 125×125 mm^2 cell area was assumed. Independent of the quality of the edge isolation groove, approximately 0.1%$_{abs}$ can be gained when the groove is moved very close to the edge. Provided that the laser accuracy is sufficient, this seems to be very attractive as the efficiency improvement comes at no extra cost.

3.3. Optimum laser groove

In an industrial solar cell on decent material with well dialed-in processes, one of the main fill factor loss mechanisms is the increased edge recombination. So, a strong effect on efficiency can be expected from a decrease in j_{0H} via the optimization of the laser parameters. This has been done as indicated by the values extracted from experimental cells in Table 1. By adjusting the laser frequency and scanning speed, we could reduce j_{0H} from 1.40 to 1.15e−7 A/cm, which translated to an efficiency improvement of ~0.2%$_{abs}$. This is supported by the simulation results shown in Fig. 6 where the value of j_{0H} has been varied from very low values corresponding to edge cleavage (1e−8 A/cm) to those expected from very damaging laser parameters ($>3e-7$ A/cm). It can be concluded from the graph that the potential for efficiency increase can easily reach the order of 0.5%$_{abs}$ and should be exploited by careful tuning of the laser parameters. Possibly the waterjet-guided laser can give superior performance in this aspect as already reported in a small study [3].

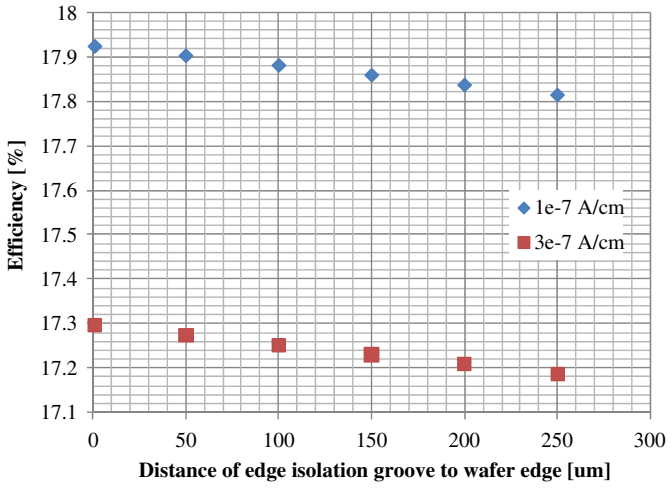

Fig. 5. Effect of moving the edge isolation groove close to the wafer edge. The dark saturation current density of the edge diode was varied.

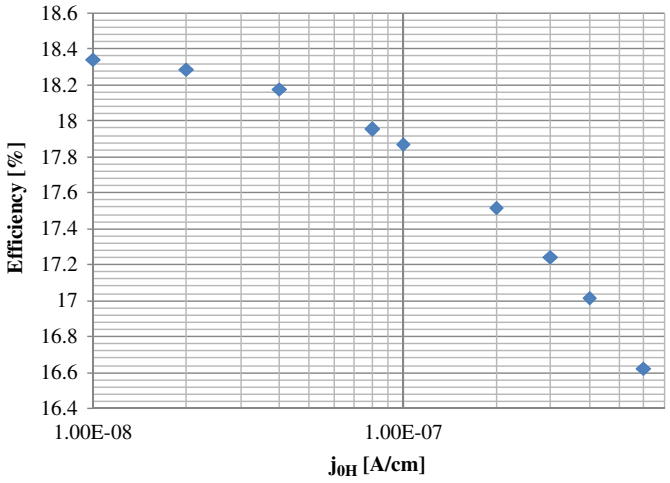

Fig. 6. Simulation results for varying dark saturation current densities at the edge region j_{0H}.

4. Conclusion

In this paper, an analytic model for the description of the series resistance of the edge region in an industrial solar cell as well as an estimation of the current generation in that region is presented. An equivalent circuit model allows for analytic calculation of cell performance depending on the edge geometry and recombination properties. It is shown that the increased edge recombination represents a severe fill factor loss mechanism and different ways to minimize these losses are pointed out. While the geometric fine-tuning of finger length only results in small efficiency gains, moving the laser groove closer to the edge results in an increase in efficiency by ~0.1%$_{abs}$ independent of the groove quality. The largest impact and thus most interesting optimization option can be expected from the laser groove quality, i.e. the laser-induced increased recombination. From carefully chosen laser parameters and/or liquidjet-guided lasers, efficiency improvements of ~0.5%$_{abs}$ are conceivable.

Acknowledgement

D.K. would like to thank K.R. McIntosh and M.D. Abbott for fruitful discussions and J. Perkins for help with the spreadsheet.

Appendix: Series resistance contributions from the edge

Definitions:

ρ_b	Base resistivity
W	Wafer thickness
$J_{sc,i}$	J_{sc} in region i
J_{sc}	J_{sc} of main solar cell
Q_i	Current that flows from region i to region $i+1$
d	Wafer edge length
d_m	Edge length of main solar cell
d_{EI}, d_{Al}	Distance of *EI* groove/*Al* metallization to wafer edge
x_f	Finger pitch
x_e	Distance of finger tips to wafer edge
w_f	Finger width

R outer radius of equivalent half-circular region representing electron current flow in region 2+3
r_0 inner radius of equivalent half-circular region representing electron current flow in region 2+3. Equals to $w_f/2$.
A_i Area of region i
A_m Area of main solar cell

Region 1 (beyond EI)

$$P^{(p)}_{\mathrm{loss},1} = 4J^2_{\mathrm{sc},1}\frac{\rho_b}{W}\left(\frac{1}{3}dd^3_{EI} - \frac{1}{4}d^4_{EI}\right)$$
$$P^{(n)}_{loss,1} = 4J^2_{\mathrm{sc},1}\frac{\rho_b}{W}\left(\frac{1}{3}dd^3_{EI} - \frac{1}{4}d^4_{EI}\right)$$

Current injected from region 1 into region 2

$$Q_1 = 4J_{\mathrm{sc},1}d_{EI}(d-d_{EI})$$

Hole current in region 2 (between EI and Al)

Hole current purely lateral, take additional current Q_1 into account.

$$P^{(p)}_{\mathrm{loss},2} = 4J^2_{\mathrm{sc},2}\frac{\rho_b}{W}\left(\frac{1}{3}(d_{Al}-d_{EI})^3(d-2d_{EI}) - \frac{1}{4}(d_{Al}-d_{EI})^4\right) - \frac{Q_1^2}{8}\frac{\rho_b}{W}\ln\left(\frac{d-2d_{Al}}{d-2d_{EI}}\right) + J_{\mathrm{sc},2}\,Q_1\frac{\rho_b}{W}(d_{Al}-d_{EI})^2$$

$$Q_2 = Q_1 + 4J_{\mathrm{sc},2}(d_{Al}-d_{EI})(d-d_{Al}-d_{EI})$$

Hole current in region 3 (between Al and finger tips)

Assuming that *Al* is closer or at same distance to edge than finger tips

Hole current vertical, full generation at surface, linear addition of Q_2 from front to back (could be problematic, when area of region 3 becomes very small)

$$P^{(p)}_{\mathrm{loss},3} = \frac{\rho_b W}{A_3}\left(J^2_{\mathrm{sc},3}A_3^2 + \frac{1}{2}J_{\mathrm{sc},3}A_3\,Q_2 + \frac{1}{3}Q_2^2\right)$$

$$A_3 = 4(x_e-d_{Al})(d-x_e-d_{Al})$$

Electron current in region 2 and 3:

Electron current combined for regions 2 and 3, taking grid geometry into account:

(a) For $\frac{x_e-d_{EI}}{x_f} \ll 1$: straight lateral current to fingers, Q_1 added to $J_{sc,2}$ (fingers close to edge)
(b) For $\frac{x_e-d_{EI}}{x_f} \geq 1$: approximate rectangular region by half circle, radial current flow, take additional Q_1 into account (finger pitch and distance of finger tips to edge comparable)
(c) For $0 < \frac{x_e-d_{EI}}{x_f} < 1$: weigh both terms with $\Gamma\left(\frac{x_e-d_{EI}}{x_f}\right) = \frac{1}{2(\cos((x_e-d_{EI}/x_f)\pi)+1)}$.

$$A_2 = 4(d_{Al}-d_{EI})(d-d_{Al}-d_{EI})$$

$$J_{\mathrm{sc},23} = \frac{A_2J_{\mathrm{sc},2} + A_3J_{\mathrm{sc},3}}{A_2+A_3}$$

$$P^{(n)}_{loss,23,a} = \frac{2d}{x_f}\left(\frac{J^2_{sc,23}\rho_{sh}\pi}{4}\cdot\left(R^4 ln\frac{R}{r_0} - R^2(R^2-r_0^2) + \frac{1}{4}(R^4-r_0^4)\right) + \frac{Q_1^2\rho_{sh}x_f^2}{16\pi d^2}ln\frac{R}{r_0} + \frac{1}{8d}(J_{sc,23}Q_1\rho_{sh}x_f)\cdot\left(R^2 ln\frac{R}{r_0} - \frac{1}{2}(R^2-r_0^2)\right)\right) + \frac{\rho_{sh}}{d-2x_e}\left(\frac{Q_1^2}{4}(x_e-d_{EI}) + J_{sc,23}Q_1(d-2x_e)(x_e-d_{EI})^2 + \frac{4}{3}J^2_{sc,23}(d-2x_e)^2(x_e-d_{EI})^3\right)$$

$$P^{(n)}_{loss,23,b} = \frac{\rho_{sh}d(x_f-w_f)^3}{24x_f(x_e-d_{EI})}\cdot\left(\frac{Q_1x_f}{2d(x_f-w_f)} + 2J_{sc,23}(x_e-d_{EI})\right)^2 + \frac{\rho_{sh}}{d-2x_e}\left(\frac{Q_1^2}{4}(x_e-d_{EI}) + J_{sc,23}Q_1(d-2x_e)(x_e-d_{EI})^2 + \frac{4}{3}J^2_{sc,23}(d-2x_e)^2(x_e-d_{EI})^3\right)$$

$$P^{(n)}_{\mathrm{loss},23,c} = \Gamma\left(\frac{x_e-d_{EI}}{x_f}\right)P^{(n)}_{\mathrm{loss},23,b} + \left(1-\Gamma\left(\frac{x_e-d_{EI}}{x_f}\right)\right)P^{(n)}_{\mathrm{loss},23,a}$$

Main solar cell

Base current:
$d_m = d-2x_e$ edge length of main solar cell

$$P_{\mathrm{loss},p} = (J_{\mathrm{sc}}\,d_m^2)^2\frac{\rho_b W}{d_m^2}$$

Emitter current:
Assume just fingers, no busbars, lateral current flow

$$P_{\mathrm{loss},n} = J^2_{\mathrm{sc}}\frac{d\,d_m\rho_{sh}}{12x_f}(x_f-w_f)^3$$

Lumped series resistance calculation

Edge

$$R_{\mathrm{ser,edge}} = \frac{P^{(p)}_{\mathrm{loss},1} + P^{(n)}_{\mathrm{loss},1} + P^{(p)}_{\mathrm{loss},2} + P^{(p)}_{\mathrm{loss},3} + P^{(n)}_{\mathrm{loss},23}}{(Q_2 + A_3J_{\mathrm{sc},3})^2}$$

Base

$$R_{\mathrm{ser,main}} = \frac{P_{\mathrm{loss},p} + P_{\mathrm{loss},n}}{J^2_{\mathrm{sc}}\,d_m^4}$$

References

[1] M.D. Abbott, et al., Investigation of edge recombination effects in silicon solar cell structures using photoluminescence. Appl. Phys. Lett. 88 (2006) 1638–1644.
[2] M. Hermle et al., IEEE 3rd World Conference on Photovoltaic Energy Conversion, Osaka, Japan, 2003, pp. 1009.
[3] D. Kray, et al., Study on the edge isolation of industrial silicon solar cells with waterjet-guided laser. Sol. Energy Mater. Sol. Cells 91 (2007) 1638.
[4] F. Chen, et al., Contactless technique to quantify the edge-junction recombination in solar cells. Appl. Phys. Lett. 89 (2006) 263509.
[5] D.A. Clugston, P.A. Basore, Proceedings of the 26th IEEE Photovoltaic Specialists Conference, Anaheim, California, USA, 1997, pp. 207.
[6] H. Antoniadis, 34th Photovoltaic Specialists Conference, Philadelphia, PA, USA, 2009.
[7] K.R. McIntosh, Ph.D. Thesis, University of New South Wales, 2001.
[8] S.R. Wenham et al., IEEE 1st World Conference on Photovoltaic Energy Conversion, Waikoloa, Hawaii, USA, 1994, pp. 1278.
[9] M.A. Green, in: Solar Cells: Operating Principles, Technology and System Applications, UNSW, Kensington, 1986, pp. 145.
[10] O. Breitenstein, P. Altermatt, K. Ramspeck, M.A. Green, Jianhua Zhao, A. Schenk, Interpretation of the commonly observed *I–V* characteristics of c-Si cells having ideality factor larger than two, in: Proceedings of the *IV* World Conference on Photovoltaic Energy Conversion, May 7–12, 2006, Waikaloa, Hawaii, pp. 789–884.